# NUMERICAL VALIDATION OF GUST RESPONSE AND NUMERICAL ASSESSMENT OF GUST LOAD ALLEVIATION FOR 2D AEROELASTIC AIRFOIL IN TRANSONIC CONDITIONS

**Fabien HUVELIN[1], Arnaud LEPAGE[1], Charles POUSSOT-VASSAL[2]**

[1] ONERA-The French Aerospace Lab
Aerodynamics, Aeroelasticity, Acoustics Department
Châtillon, 92320 FRANCE
fabien.huvelin@onera.fr, arnaud.lepage@onera.fr

[2] ONERA-The French Aerospace Lab
Information Processing and Systems Department
Toulouse, 31055 FRANCE
charles.poussot-vassal@onera.fr

**Keywords:** Aeroelasticity, CFD, Gust response, Control law, Dynamic Coupling

**Abstract:** ONERA has designed an experimental set-up dedicated to the gust load analysis and the demonstration of active gust load alleviation in transonic flows. Two main campaigns have been performed leading to the generation of database for high fidelity tools validation. The first one was dedicated to the open-loop analysis in order to measure the airfoil response due to a sine gust for both rigid and flexible cases. The second one was dedicated to the assessment of control laws implemented for gust load alleviation. These databases have been used in order to validate and to assess the capabilities of the in-house code elsA (ONERA-Airbus-Safran property) using its aeroelastic module and a gust model based on the "Field Velocity Method".

In order to perform a physical validation as close as possible to an industrial modeling, the gust method implemented in elsA ("Field velocity Method") has to be validated with farfield boundary conditions. A validation process is defined in order to move from experimental results performed in the wind tunnel with wall boundaries to numerical results computed with farfield boundaries. The full process is applied to a transonic case (Mach 0.73) with an angle of attack of 2°. Sine gust signals with a frequency corresponding to the heave structural mode (25Hz) are chosen. Results are compared in terms of aerodynamics data (pressure distribution around the airfoil) and structural data (accelerometers located close to the leading and trailing edges).

In order to assess the capability of the code to perform gust load alleviation analyses, a control law synthesized during the experimental campaign is implemented in the code. At each time step, the acceleration computed from the structural solver is sent to the control law which computes a flap deflection. The deflection is applied to the mesh and the aeroelastic problem is solved. In order to evaluate the code capabilities, two computations are performed: one with and one without the active closed-loop control law. A comparison of the acceleration data is carried out, in order to validate the capability of the code to alleviate the gust with a control law.

## 1 INTRODUCTION

Under the European Union's (EU) Clean Sky Joint Technology Initiative (JTI) program, ONERA was involved in the Load Control work package of the Smart Fixed Wing Aircraft (SFWA) project. The work package aimed at developing technologies that enable a global assessment of new devices, architectures and control laws for Load Control [1], [2]. Under this work package, ONERA intended to deal with the gust load case, which is one of the most critical for strength design and fatigue loading source for transport type aircraft. In the investigation of gust loads, it is required to have relevant experimental data to validate the models and analyze that will serve to design innovative control approaches and prove the ground efficiency. In academic or industrial research area, there are few works conducted on the experimental investigation of gust in wind tunnel, especially for the transonic regime. Studies have been performed in low speed regime based on various mechanisms for creating an oscillating flow in a wind tunnel: experiments based on rotating slotted cylinder [3] or composed of oscillating airfoils [4]. In the transonic speed range, very few wind tunnel experiments can be identified: concepts based on oscillating vanes [5] or using a single pitching airfoil [6] have been recently built in transonic wind tunnel environments. But considering these studies, there is still a lot of work to perform in order to improve the understanding of the physical phenomena involved in fluid structure interaction with a gust perturbation and therefore to improve the definition of gust load alleviation strategies. To achieve the experimental investigation, ONERA proposed to define a research tool for the investigation of gust load in Wind Tunnel (WT) tests conditions. The key objectives for ONERA were:

- To improve the understanding of a large scope of physical phenomena induced by a gust such as linear and non-linear aerodynamics in presence of gust, aeroelastic effects of the impact of a gust on a flexible model,
- To dispose of comprehensive and relevant experimental databases for the validation of methodologies and tools of numerical simulation such as high fidelity tools of Computational Fluid Dynamic (CFD).
- To investigate gust load alleviation with control approaches based on closed-loop architecture.

This paper focuses on the numerical aspects. ONERA has implemented in the elsA software the capability to compute the high fidelity aeroelastic gust response, directly in time-domain, for different discrete gust shapes. First, this paper deals with the ability of elsA to restitute an appropriate gust response around a flexible airfoil for transonic conditions and for different sinusoidal gust shapes by comparing numerical computations with the Field Velocity Method and experimental results. Second, the capability to perform a simulation of gust load alleviation with control law given by experimental database is assessed.

## 2 WIND TUNNEL TEST CAMPAIGNS

### 2.1 Experimental set-up

The experimental set-up is composed of a gust generator and an aeroelastic model (Figure 1). The purpose of the gust generator is to dispose of an experimental tool able to generate relevant perturbations (gust load) for wind tunnel conditions from subsonic to transonic conditions. The concept of the gust generator is composed of two movable 2D wings fixed on the walls of the wind tunnel. The gust generator is located upstream the wind tunnel test section and its functioning is based on a synchronous motions of the 2 airfoils (pitch dynamic motions). This architecture allows generating a gust field downstream the test section.

The aeroelastic model aims at representing the behavior of a classical 2 degrees of freedom (dof) aeroelastic model. The main objective is to define an aerodynamic part of the model (the airfoil in the test section) as rigid as possible in order to preserve the 2D characteristic of the flow around the model. The desired rigid-body heave and pitch modes respectively consists in vertical translation and rotation around a specific axis. For each degree of freedom, the frequency of the corresponding mode (heave mode or pitch mode) is completely determined by a couple of stiffness and mass (or inertia) parameters. In the wind-tunnel test section, the global 2dof mounting system is composed of 2 identical mountings parts located on each test section door. On both sides, the wing part is attached to the 2dof system at each wing root by a connection to the pitch shaft. The device includes also mechanical stops to limit dynamic motions in case of too high oscillation amplitude. Moreover the pitching device allows modification of the wing model angle of attack in a large range. The OAT15A airfoil designed by ONERA [7] is selected as the aeroelastic model in order to evaluate the response to a gust load. It is representative of a supercritical airfoil for transport aircraft. The design point is at Mach number M = 0.73 for a lift coefficient of Cl = 0.65 and the thickness to chord ratio of the airfoil is 12.3%. The model has a 250 mm chord and a 3.2 aspect ratio. As one of the main objectives of the experimental roadmap is to performed active gust load alleviation, the model needed to dispose of a control mean. The choice of a full span trailing edge control surface is made to preserve as much as possible the two-dimensional behavior of the flow. The hinge axis is located at 75% of the chord.

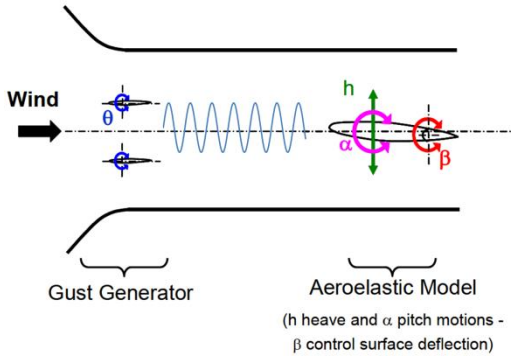


Figure 1: Sketch of the experimental set-up

Tests have been performed in the ONERA S3Ch research wind tunnel located in the ONERA Meudon Center (Figure 2). This closed return wind tunnel is a transonic continuous run facility with a 0.8m x 0.8m square test section for a 2.2m length. It covers a Mach number range from 0.3 to 1.2 and operates at atmospheric stagnation pressure. The top and bottom walls of the test section can be either rigid walls or deformable adaptive walls. In the latter case, the wall displacements are estimated in order to adapt the steady flow in the model area by minimizing the wall interferences.

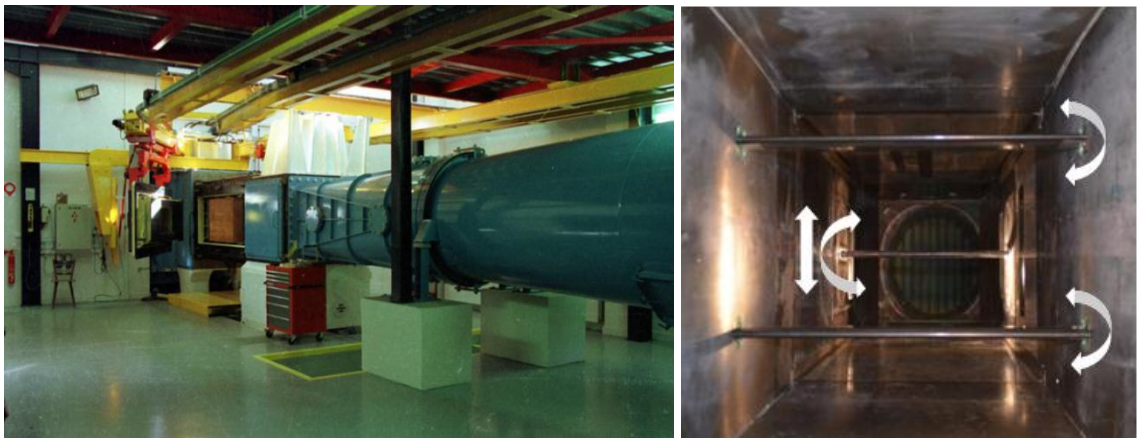

Figure 2: ONERA S3Ch wind tunnel and “Inside view” of the experimental set-up of the second wind tunnel test: the gust generator (foreground) and the aeroelastic model (background)

### 2.2 Instrumentation

In order to generate an experimental database for the validation of high fidelity numerical codes, different measurement techniques are selected for the wind tunnel tests. The main part of the instrumentation is made of steady and unsteady pressure transducers arranged in two span stations: one steady and one unsteady pressure measurements sections. As the Wind Tunnel is not equipped with external force balance, the estimation of aerodynamic forces and moment can be estimated by integrating the pressure distributions. Additionally, the model is equipped with accelerometers mounted in three span stations in order to correctly handle the dynamic motions for both flexible and rigid motions and for the wing and control surface parts. The main embedded instrumentation is composed of 44 unsteady pressure sensors (Kulite), 31 steady pressure sensors (Pressure Tabs) and 12 Accelerometers. Gust measurements are performed with an unsteady clinometric probe specifically designed for these tests. This “gust sensor” allows the investigation of the unsteady flow field downstream in the test section for different aerodynamic conditions and for different control signals of the oscillating airfoils. It is located on the right side in the spanwise direction in order to avoid any 3D flow disturbance on the center line of the airfoil.

## 3 NUMERICAL TOOLS

### 3.1 CFD/CSM numerical tool

The high fidelity simulation tool developed at ONERA for aeroelastic applications is based on the elsA CFD solver (ONERA-Airbus-Safran property) for the flow computation [8], [9]. A general framework has been developed in the optional “Ael” subsystem of elsA over the last decade, giving access in a unified formulation to several types of aeroelastic simulations, while minimizing the impact on the flow solver. The available simulations cover nonlinear and linearized harmonic forced motion, steady aeroelasticity and dynamic coupling simulations in time-domain with different structural modeling approaches. The motivation of these developments, detailed in [10], [11], [12] is to provide a numerical tool for the prediction of various aeroelastic phenomena such as flutter or LCO and aerodynamic phenomena involving complex nonlinear flows such as shocks, vortex flow, and flow separation. An overview of the coupled simulation system is shown in Figure 3.

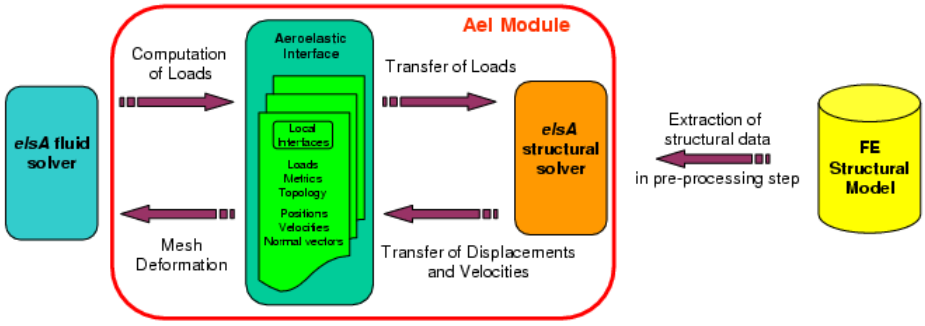


Figure 3: Aeroelastic optional subsystem of **elsA** for aeroelastic simulations

### 3.2 Methodology for dynamic coupling

Dynamic coupling simulation capabilities have been developed on the elsA platform in the case of a modal approach for the structure. The numerical technique is based on an iterative process which is converged at each physical time-step. The different steps which are performed at each time step are, (Figure 4):

1. Computation of the flow solution
2. Computation of the generalized aerodynamic loads (GAF)
3. Computation of the generalized coordinates, solving the mechanical modal system
4. Computation of the displacements of the aerodynamic surface grid, from the modal shapes and the generalized coordinates
5. Deformation of the aerodynamic grid

Dynamic coupling has been developed in **elsA** when the flow computation makes use of the dual time-stepping technique (step1), allowing the use of large physical time-steps. The generalized aerodynamic loads are then computed from (step 2):

$$gaf_i = \iint_{Wall} -p\,\vec{n}\,\vec{\Phi}_{A,i}\,dS \qquad (1)$$

where $\vec{\Phi}_{A,i}$, i=1,N are the N first mode shapes, mapped on the aerodynamic surface grid.

The mapping $\vec{\Phi}_{S,i} \Rightarrow \vec{\Phi}_{A,i}$ from the structural grid to the aerodynamic surface grid is achieved in a preprocessing step, using the same interpolation or fitting techniques as those used for static coupling. The generalized coordinates $q_i$ are computed, in step 3, from the dynamic modal system, using the implicit Newmark scheme for time discretization:

$$m_i \ddot{q}_i + 2 m_i \alpha_i \omega_i \dot{q}_i + m_i \omega_i^2 q_i = gaf_i \quad (i = 1, N) \qquad (2)$$

where $m_i$ is the generalized mass, $\omega_i$ the pulsation, and $\alpha_i$ the structural damping coefficient.

The wall displacements and velocities, $\Delta\vec{X}_A$, and $\Delta\dot{\vec{X}}_A$ are provided directly on the aerodynamic surface grid by:

$$\Delta \vec{X}_A(M,t) = \sum_{i=1}^{N} q_i(t)\vec{\Phi}_{A,i}(M), \qquad \Delta \dot{\vec{X}}_A(M,t) = \sum_{i=1}^{N} \dot{q}_i(t)\vec{\Phi}_{A,i}(M) \tag{3}$$

The deformation of the aerodynamic grid (step 5) is performed differently with respect to the static coupling case, taking advantage of the modal approach used for the structural computation. An individual "modal mesh deformation" is first computed for each mode at the start of the coupled simulation, using one of the two techniques available in **elsA**. The instantaneous mesh deformation $\Delta \vec{X}_A^n$ at time level n is then computed as a linear combination of these individual "modal" mesh deformations:

$$\Delta \vec{X}_A^n = \sum_{i=1}^{N} q_i^n \Delta \vec{X}_{A,i}^{modal} \tag{4}$$

where $q_i^n$ are the generalized coordinates solution of the dynamic modal system.

Additional steps are performed when the flow computation makes use of the Chimera technique (yellow boxes in Figure 4). These additional steps are performed to avoid a double counting of loads in overlapping regions, and are based on the use of the USURP software developed by Pennsylvania State University.

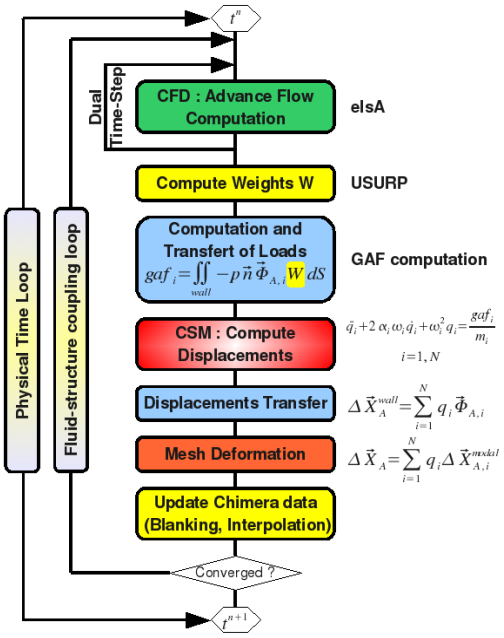


Figure 4: Fluid-structure modal dynamic coupling diagram

### 3.3 Gust modeling and implementation

There are several possibilities in order to implement a gust perturbation in CFD codes. One way consists in introducing the gust velocity in the far field boundary conditions of the computational domain. This approach would allow not only taking into account the effect of the gust on the aircraft, but also the reverse effect of the aircraft on the gust. However, the main problem of such an approach is that the gust must in this case be propagated from the boundaries of the computational domain to the aircraft location, without being damped by the numerical dissipation of the discretization schemes. This would require high order schemes and also the use of fine grids in a large part of the computational domain.

An alternate approach is to use the so-called “Field Velocity Approach” suggested by Sitaraman et al [13]. This latter takes advantage of the Arbitrary Lagrangian Euler (ALE) formulation., It introduces a grid velocity in the Navier-Stokes equations, allowing the taking into account in a consistent way of the mesh deformation in the numerical simulation. In the “Field Velocity Approach”, a prescribed gust velocity field, depending on both space and time, is added to the grid deformation velocity in each cell of the aerodynamic grid. The so-called “geometric conservation law” (GCL) is moreover used with the ALE formulation, and allows to maintain a conservative numerical scheme, and to avoid additional numerical dissipation. The field velocity approach has been implemented in the ONERA tool **elsA-Ael** [14], [15]. Three models of discrete gust have been implemented (Figure 5):

- The “sharped edge gust” signal;
- The “one-minus cosine” signal, often used for certification;
- The “sine” signal which could be used for the simulation of harmonic gust response.

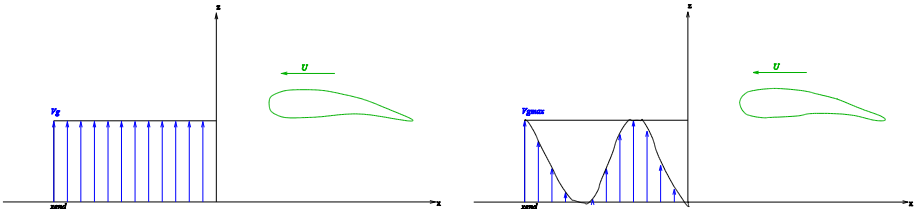

Figure 5: Sharp edge (left) and harmonic sine (right) gust signal implemented in elsA

## 4 NUMERICAL MODEL

### 4.1 Test campaigns analysis for numerical restitution

Three wind tunnel test (WTT) campaigns have been achieved:

- The first campaign in the ONERA S3Ch wind tunnel aimed at estimating whether this device made of two oscillating airfoils was able to generate a relevant gust field.
- The second WTT was dedicated to analyze the effects of impacting gusts on the aeroelastic model behavior for different aerodynamic conditions (both subsonic and transonic). Three kinds of open-loop test have been performed: gust impacting a rigid airfoil; gust impacting an aeroelastic airfoil; aileron motion with aeroelastic airfoil and without gust. These tests allowed the characterization of the aeroelastic response of the model to gust and aileron motion.
- The third WTT was dedicated to gust control. Based on the open-loop results, a robust control law have been synthetized (with a damping attenuation objective) and tested in the wind tunnel.

From the first WTT, the results analysis leads to the following conclusions:

- The ability to generate a reproducible and significant gust field in a wind tunnel environment has been proved. Especially, the gust produced by the generator can be modeled as a sine signal;
- The steady and unsteady pressure sensors around the airfoil placed at two different locations along the span allow validating the fact that phenomena around the airfoil can be considered as two-dimensional.

From the second WTT, the analysis of results for both rigid and flexible model conditions leads to the following conclusions:

- A small deflection appears on the flap due to the static loads. It is therefore measured with an optical process based on photogrammetry measurements (the uncertainty on the measurements is assumed negligible);
- The uncertainty on the measurement of the steady value of the angle of attack can be neglected in wind-off conditions;
- The uncertainty on the measurements of deformable adaptive walls is assumed negligible;
- In the aeroelastic response of model, 3D components were observed in the steady deformation state (dominated by the heave and pitch modes including also bending components).

From a modeling point a view:

- The results analysis allows considering computations with a 2D-model;
- The targeted steady flap deflection was updated with the estimated value during tests thanks to the measurements provided by the optic device;
- In order to take into account the 3D bending at steady state, a solution is to modify the wind-off angle of attack. Due to the uncertainty on this variable, a full 2D model of the wind tunnel has to be built in order to evaluate its value. So, wind-off angle of attack is considered as an unknown and is assessed during the steady state computation;
- The temperature at boundaries is assumed constant, so no uncertainty on the inlet enthalpy is taken into account;
- The wall deformations experimentally measured have been used in order to deform the mesh with the assumption that the uncertainty on the measurements can be neglected.

### 4.2 Computation process

In order to perform a computation as close as possible to an industrial modeling, the "Field velocity method" must be validated with farfield boundary conditions. A validation process has to be defined in order to move from experimental results performed in the wind tunnel with wall boundaries to numerical results computed with farfield boundaries.

Firstly, the numerical options have to be checked by comparing results with similar modeling. The WTT campaign analysis leads to perform steady computation on the 2D full model of the wind tunnel in order to assess the wind-off angle of attack and numerical options used for steady computation. Comparisons focus on the averaged pressure field around the airfoil. The parameters used in order to adjust the boundary conditions and the wind-off angle of attack are: the data provided by a pressure probe located at the beginning of the test section and the shock location on the airfoil.

Secondly, unsteady computations on the 2D full model validate the corresponding numerical options by comparing the pressure signals of the unsteady pressure sensors around the airfoil and accelerometers located close to the leading and trailing edges.

Thirdly, based on the airfoil position estimated during the first step and the corresponding numerical options, the steady state conditions for a farfield modeling have to be assessed. Aerodynamic conditions are adjusted in order to get the required shock location.

Finally, the unsteady computations with farfield boundaries are computed with the Field Velocity Method. The gust amplitude is tuned in order to reach the gust amplitude experimentally measured at the gust probe location.

For the unsteady cases, the same post-processing based on Fast Fourier Transform is applied to the experimental and numerical pressure signals in order to perform consistent and reliable comparison.

### 4.3 Wind-off angle of attack identification

For the first step of the computation process, an identification method has been defined in order to assess the wind-off angle of attack. The following sensors are used as target parameters: the shock location on the airfoil and the probe located after the throat which drives the aerodynamics conditions (Mach and static pressure) in the wind tunnel. The wind-off angle of attack, combined to the inlet and outlet pressure in the wind tunnel, are tuned until the convergence of the target parameters to experimental values (Figure 6). The problem is formulated with cost functions and is solved with a Newton-Raphson algorithm.

The same approach is used for the third step in order to assess the aerodynamic conditions for the farfield modeling. The problem is easier because the only unknown parameter is the Mach number and the corresponding target parameter is the shock location.

For the fourth step, the gust amplitude behavior is quite linear. The FVM amplitude to be prescribed in the numerical simulations is driven by the gust amplitude level estimated during WTT at the gust probe location.

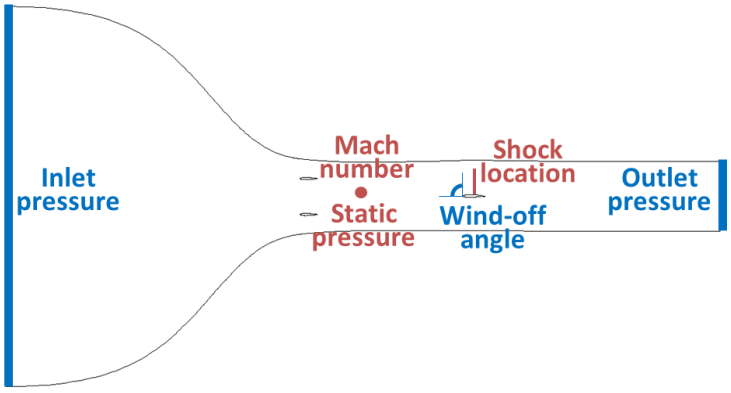


Figure 6: Wind-off angle identification: unknown parameters (blue) and target parameters (red)

### 4.4 Options for simulation

A steady set of parameters has been defined during the first step for the computation process and an unsteady set of parameters set during the second step.
The fluid is assumed to be a viscous perfect gas. The Wilcox (k,ω) turbulence model is used with the Zheng limiter.

Experimental structural modes of the airfoil have been identified experimentally in the Wind Tunnel test section. Only, the structural sensors located along the center line in spanwise direction have been used in order to smooth the mode on the aerodynamic mesh. A linear smoothing has been applied, as preprocessing, from the structural sensor to the aerodynamic mesh.

The backward Euler scheme is used for time integration. For unsteady simulations, the Dual Time Step technique is chosen. The time step is computed depending on the gust frequency and the number of iterations per gust period chosen (between 16 and 128 during the time step sensitivity analysis). 100 dual-iterations per time step are imposed. The Jameson centered flux scheme is used with a scalar artificial viscosity. The $2^{nd}$ order dissipation coefficient (k2) is set to 0.5, the $4^{th}$ order dissipation coefficient (k4) is set to 0.032. For viscous fluxes, gradients are computed at cell centered (5-point stencil), corrected to remove even-odd decoupling. A V-cycle multigrid procedure is imposed with 2 coarse grids. The dissipation coefficients used on the finest grid are also used on the coarse grids.

The mesh is deformed with the Transfinite interpolation method. For the steady computation, no relaxation is imposed for the coupling step. The fluid and the structure are coupled every 200 iterations. For the unsteady computation, the fluid and the structure are coupled 4 times per time step. So, 25 sub-iterations of the aerodynamic solver are performed between each fluid-structure coupling.

### 4.5 Meshing

Two models are built: one for the wind tunnel test conditions and one for the farfield conditions.

The wind tunnel is modeled in 2D (Figure 7). It takes into account the two wings of the gust generator, the OAT15 airfoil and the upper and lower walls of the wind tunnel. In order to avoid any numerical approximation due to no-match or Chimera conditions, all block interfaces are matched. A condition of adherent wall is imposed on each wall of the domain (upper and lower walls, airfoils). These constraints lead to a first mesh built with 316000 cells in the domain, 192 nodes on each side of the OAT15 airfoil and 100 nodes on each side of each gust generator. From this mesh, a second one is built by applying a refinement by a factor 2 along each direction. It leads to a mesh with 1.25 million of cells.

The OAT15 airfoil is modeled with farfield conditions and conditions of adherent wall on the airfoil (Figure 7). A C-mesh is built around the airfoil leading to a mesh of 99 000 cells with 207 nodes on each side of the airfoil. From this mesh, two refined meshes are built by applying, respectively, a refinement by a factor 2 and 3 along each direction. It leads to meshes with 396000 cells and 891000 cells.

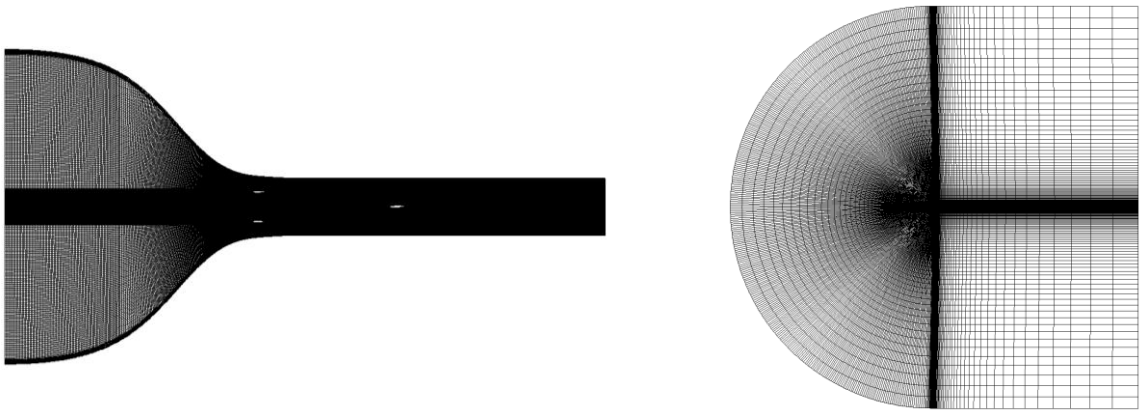

Figure 7: Wind tunnel mesh (left) and farfield mesh (right)

# 5 CASES VALIDATION

## 5.1 Case definition

Tests are performed at Mach number 0.73 with an angle of attacks (AoA) of 2°. The restitution case corresponds to a sinusoidal excitation at 25 Hz (closed to the first structural mode of the model) induced by a dynamic motion of +/-3° of the gust generator wings leading to a gust angle of +/-0.21° close to the airfoil.

## 5.2 Wind tunnel modeling

From the first step of the computation process, the wind-off angle is assessed based on the Mach number and static pressure given by the wind tunnel pressure probe and based on the shock location estimated by pressure sensors located on the airfoil. The wind-off angle identification algorithm is launched until a relative convergence on the three target parameters less than $10^{-10}$ is achieved. A mesh sensitivity analysis is performed on two mesh refinements. The mesh sensitivity analysis shows that the two levels of refinement give the same wind-off angle (1.43°) and pressure distribution (Figure 8). Comparing the numerical and experimental data, on the upper surface a difference appears at the shock root. Numerical results under-estimate the pressure on the upper surface. On the lower surface, the pressure is over-estimated.

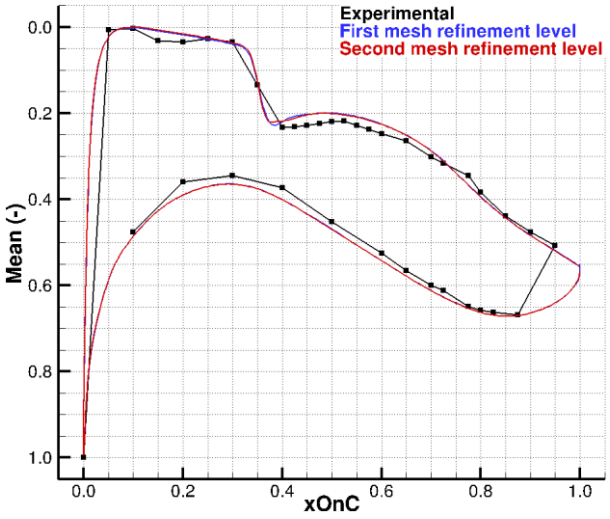


Figure 8: Pressure distribution around the OAT15 airfoil (Farfield modeling)

For the unsteady computation with wind tunnel modeling (step 2), the mesh sensitivity study is performed on two levels. For both meshes, time step sensitivity is studied with 4 levels of refinement. The gust sine signal is discretized with respectively: 16, 32, 64 and 128 iterations per period.

First of all, the space and time sensitivities are evaluated on the gust probe location. The clinometric probe is located 0.08 m ahead of the leading edge. The gust velocity vector is post-processed at each time step in the closest cell to the experimental location in order to obtain a dynamic gust angle. Due to the aeroelastic deformation, the clinometric probe location changes during the simulation. In order to have an accurate assessment of the gust velocity, it is assumed that the clinometric probe has a rigid motion. A Fourier analysis is applied on the gust velocity in order to get the module corresponding to the frequency applied on the gust generators. The space and time discretization have no influence on the gust

module. The numerical gust module (0.27°) is over-estimated in comparison with the experimental value (0.21°).

Based on the numerical sensitivity analysis, a good compromise between results convergence and time and space refinement leads to the selection of the second mesh level with 64 iterations per periods. From an aerodynamic point of view, the pressure around the airfoil is post processed with a Fourier analysis. The gust velocity at the clinometric probe, as explained above, is used as reference for the Fourier analysis. From an aerodynamic point of view, the main phenomena are caught (Figure 9). The differences are:

- The maximum amplitude is more important for the numerical computation. As seen previously, the gust velocity computed at the clinometric probe is more important than the experimental measured value. This could be the reason of the difference of maximum amplitude for the module distribution;
- The simulation underestimates the module on the lower surface like for the steady state (Figure 8);
- At the shock root, the module and the phase are not well restituted. The steady computation shows already a small over-estimation at this location.

From a structural point of view, a similar post-treatment is applied on the acceleration around the airfoil. The acceleration around the airfoil is built from the mode shape and the generalized acceleration given by the simulation. The gust velocity is also used as reference for the Fourier analysis. The main phenomena are also caught (Figure 10). The differences are:

- The main difference appears on the module close to the leading edge with an over estimation;
- Close to the flap hinge, the module variation is not well predicted. The simulation gives a mean value between the 3 sensors values. The main rigid motion of the airfoil might have modified by local gaps or deformations in the hinge area;
- A small difference appears also on the phase.

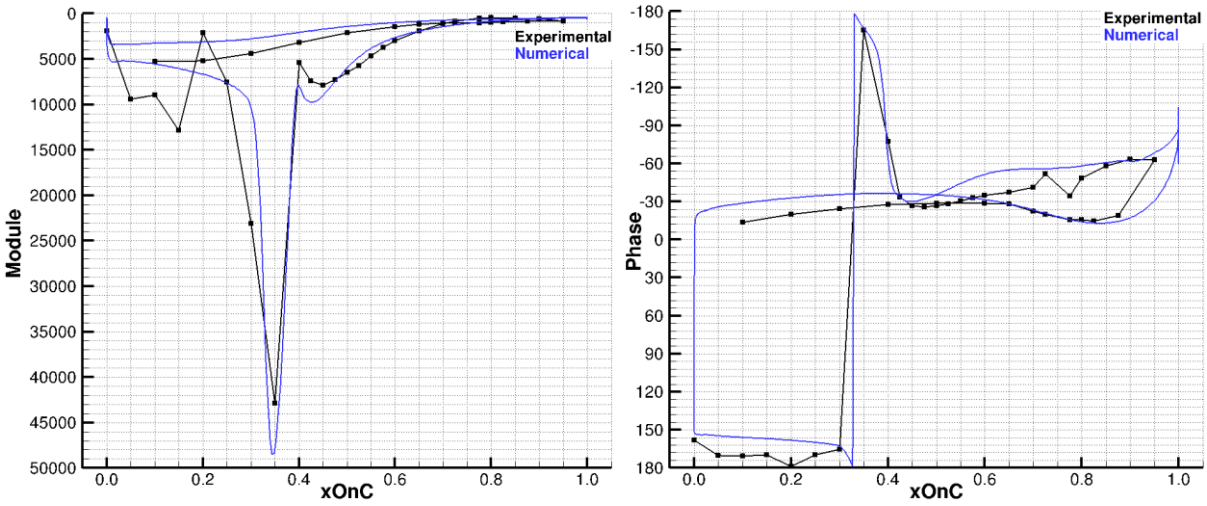


Figure 9 : Aerodynamics - Comparison of numerical and experimental results - Module (left) and phase (right) distribution around the OAT15 airfoil (wind tunnel modeling)

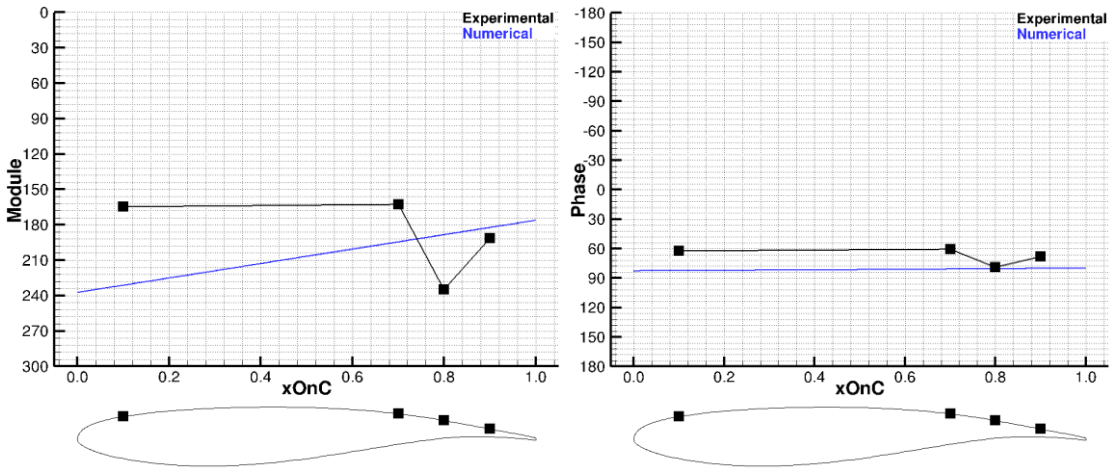


Figure 10: Structure - Comparison of numerical and experimental results - Module (left) and phase (right) distribution around the OAT15 airfoil (wind tunnel modeling)

### 5.3 Farfield modeling

From the third step of the computation process, the aerodynamics conditions found during the first step are re-imposed (wind-off angle of attack). A correction on the Mach number has to be added in order to take into account the farfield conditions. The Mach number is assessed based on the shock location given by the static pressure probe located on the airfoil and the wind-off angle of attack assessed during the first computation step. The identification algorithm is launched until a relative convergence on the target parameter less than $10^{-10}$. The mesh sensitivity analysis is performed on three mesh refinements. The mesh sensitivity analysis shows that the three levels of refinement give the same Mach number (0.72) and pressure distribution (Figure 11). Comparing the numerical and experimental data, the pressure distribution is well reproduced except after the shock root. As for the wind tunnel modeling, the pressure distribution is under estimated. The lower surface is better predicted than in the case of the wind tunnel modeling. The three levels of refinement give the same static pressure distribution around the airfoil.

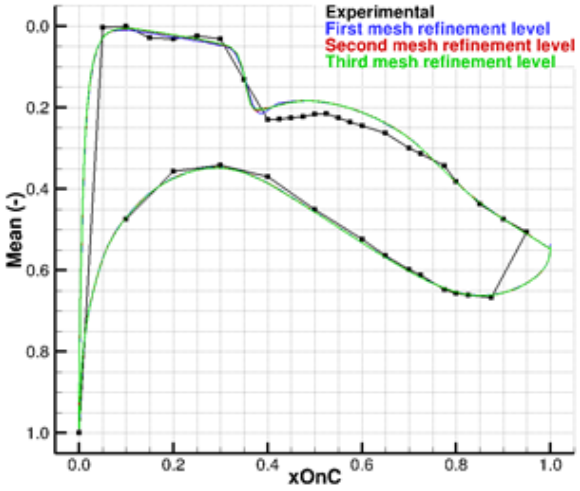


Figure 11: Pressure distribution around the OAT15 airfoil (Farfield modeling)

As for the steady computation, the mesh sensitivity study, for the gust response simulation, is performed on three grid refinement levels. For all meshes, time sensitivity is studied on 4 levels. The gust sine signal has been discretized with respectively: 16, 32, 64 and 128

iterations per period. For the Field Velocity Method, the gust magnitude at the clinometric probe location depends on the magnitude imposed to the Field Velocity Method. Due to a relative linear behavior between the values imposed in the model and the values computed at the gust location, two computations are performed in order to assess the magnitude to be imposed using the Field Velocity Method. From the sensitivity analysis, the second grid level of refinement with 64 iterations per period is selected for comparison with the experimental data.

The aerodynamics is restituted with more difficulty than the wind tunnel modeling (Figure 12). On the one hand, the module peak is well caught, due to the tuning of the FVM model. On the other hand, the module after the shock root and on the lower surface is less accurately predicted. A large difference appears on the phase around the trailing edge. The wind tunnel modeling leads to a better prediction of the phase.

The structural behavior is better restituted with the farfield condition than with the wind tunnel modeling (Figure 13). With the farfield modeling, the module is closer to the experimental result near the leading edge. A small difference appears near the trailing edge. The phase is accurately predicted.

Comparing both modeling, the farfield modeling gives a better restitution of the structural response while the wind tunnel modeling gives a better restitution of the aerodynamics. The same structural data and solver are used in both cases. Therefore the difference on aeroelastic results comes from the aerodynamics. For the boundary conditions modeling, the wind tunnel walls are deformed in order to reduce their impact on the flow around the airfoil. Two other main differences appear between the modeling approaches which could explain the deviation:

- For both cases, a constraint is to catch the shock location. The consequences for the wind tunnel modeling are to under-estimate the pressure distribution after the shock root and to over-estimate the pressure on the lower surface. For the farfield modeling, the consequences is to under-estimate more largely the pressure distribution after the shock root but to have a better estimation of the pressure on the lower surface.
- The gust amplitude is adjusted for the farfield modeling in order to have the same maximum amplitude at the clinometric probe location.

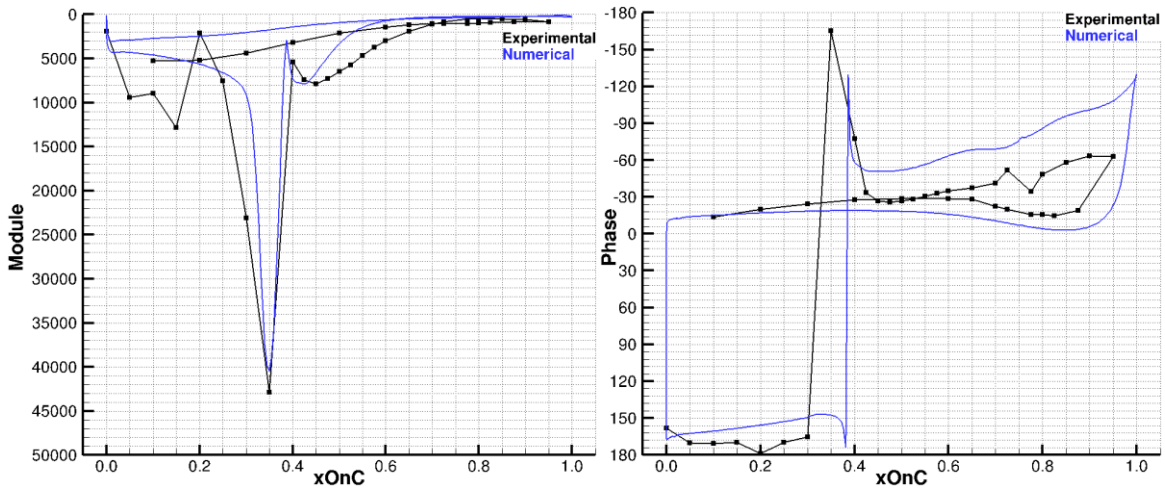


Figure 12: Aerodynamics - Comparison of numerical and experimental results - Module and phase distribution around the OAT15 airfoil (Farfield modeling)

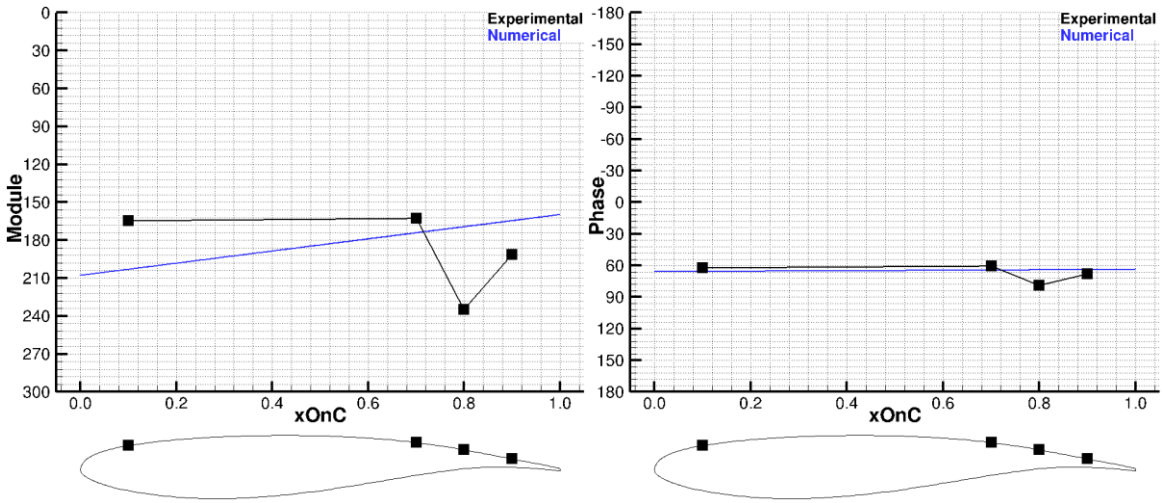


Figure 13: Structure - Comparison of numerical and experimental results - Module and phase distribution around the OAT15 airfoil (Farfield modeling)

## 6 CONTROL LAW IMPLEMENTATION IN ELSA

In order to alleviate the gust impacting the airfoil, a feedback control system is used (Figure 14). This system tends to maintain the acceleration as close as possible to zero by adapting the flap deflection. The control law is built in two steps ([16], [17]):

- First, the system behavior (P) identification is performed during the second WTT campaign (open-loop test campaign) based on flap command inputs and for various aerodynamic conditions. Two advanced frequency-domain methods are successfully used for obtaining the state space model (P): one grounded on the Loewner interpolation and the other, based on an innovative subspace formulation including eigenvalues constraints based on LMI regions.
- Second, a dynamical controller (K) is defined by using robust synthesis tools and by minimizing the $H_\infty$ norm of the frequency response function.

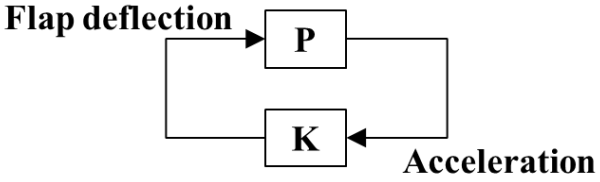


Figure 14: Generalized control scheme

From a numerical point of view, the following problem has to be solved:

$$\begin{cases} \theta_{flap}^{n+1} &= \alpha \bar{\bar{S}}^{n+1} \ddot{X}_{probe}^{n+1} \\ \bar{\bar{S}}^{n+1} &= S(\bar{\bar{S}}^{n}, \ddot{X}_{probe}^{n+1}) \end{cases} \tag{5}$$

With $\ddot{X}_{probe}$ the acceleration at a given accelerometer, $\theta_{flap}$ the flap deflection, $\alpha$ the control law gain, $\bar{\bar{S}}$ the control law represented as a matrix system. At each coupling step between the aerodynamics and the structure, the acceleration computed from the structural solver is sent to the control law which computes a flap deflection. The deflection is applied to the mesh and the aeroelastic problem is solved (Figure 15).

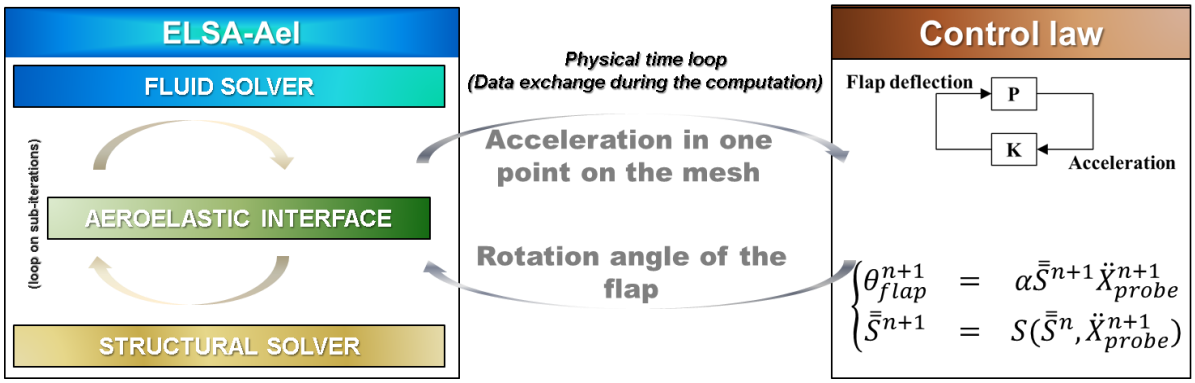


Figure 15: Aeroelastic high fidelity solver and control law coupling

In order to evaluate the code, two computations are performed: one with and one without the control law, the concerned control filter was tested successfully during the WT tests. The same aerodynamics and aeroelastic conditions than for the validation step are used. A comparison is made on the acceleration in order to validate the capability of the code to alleviate the gust with a control law. The activation of the control law (Figure 16) shows a large reduction of the acceleration extremums with the same magnitude order than the experimental results in terms of relative reduction. The flap deflection varies in a range of +/- 4° in order to counteract the sine gust, while for the experimental results the range was closest to +/- 1° [16]. As expected, a lower gain reduces the law efficiency while a higher gain leads to loss of efficiency with an acceleration increasing (Figure 17). So, the numerical coupling has the same behavior than the experimental test validating the coupling of a control law with the high fidelity code.

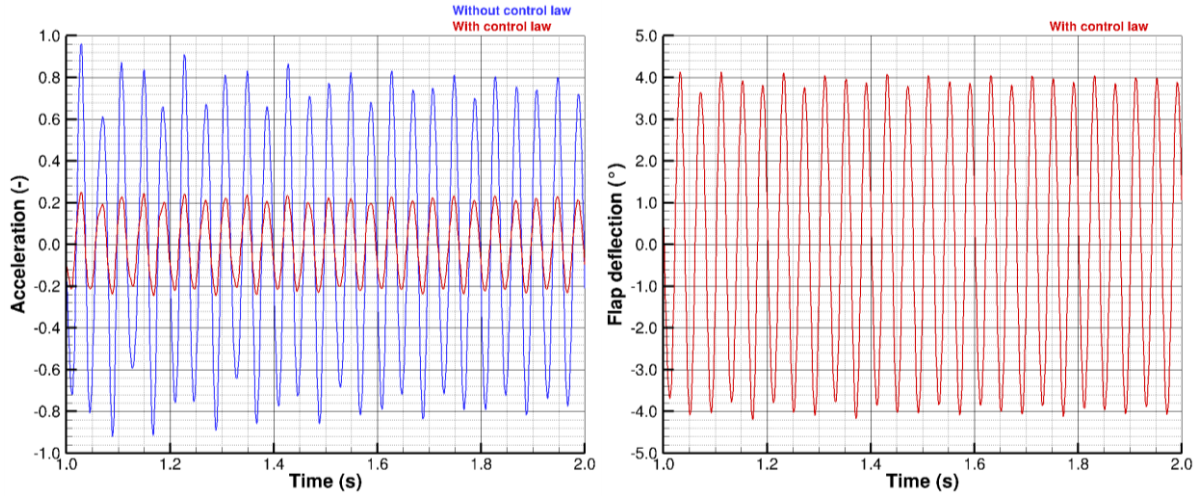


Figure 16: Acceleration comparison with and without control law (left) – flap deflection with control law (right)

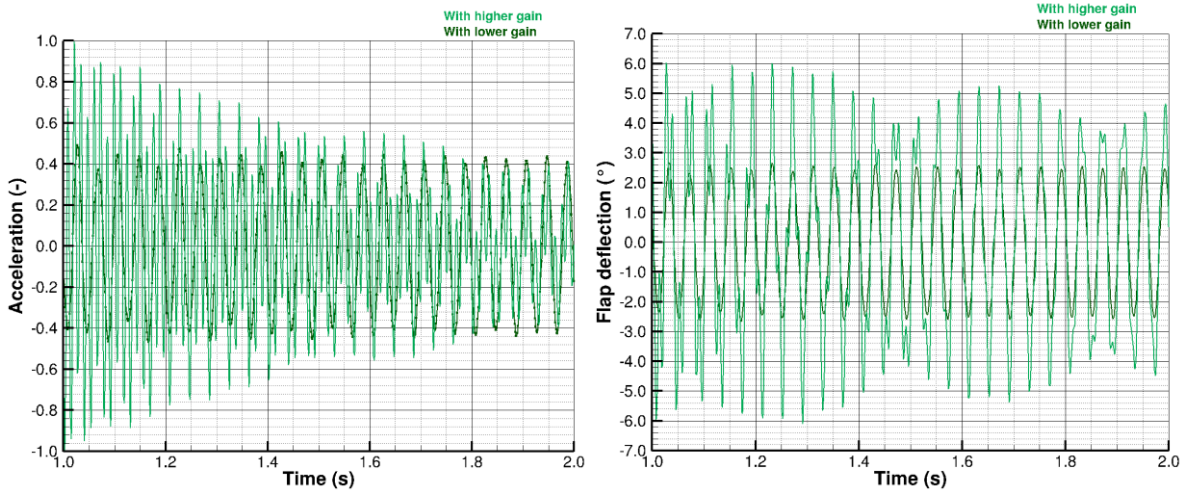


Figure 17: Gain amplification impact - acceleration (left) and flap deflection (right)

## 7 CONCLUSIONS

A physical validation of gust sine response has been performed with the in house high fidelity code elsA for aeroelastic response simulation in transonic flows. A sinusoidal gust perturbation closed to the modal frequency of the first mode of the model (heave mode) has been chosen as study case. A sensitivity analysis in space and time has been performed and allowed the selection of the appropriate refinement level. Firstly, the numerical options have been validated thanks to the modeling of the full wind tunnel test. Secondly, the capabilities of the Field Velocity Method have been assessed with farfield boundary conditions. The aerodynamics field has been fit by adjusting the wind-off angle of attack due to a 3D bending mode. The numerical simulations have demonstrated that aerodynamic and structural behaviors induced by gust are well reproduced. The main difference between the experimental and numerical results appears for the phase with the farfield modeling. In order to improve the restitution and to better understand the phenomena, a 3D modeling of the wind tunnel could be useful in order to take into account the 3D deformation effects of the structure (i.e.; 3D bending).

In a second step, a closed-loop simulation has been performed. An experimental control law has been coupled to the high fidelity code. The maximum alleviation obtained is similar to the one obtained experimentally. Tests on the control law behavior by changing the gain factor leads to the expected results. The work achieved so far shows that the progress and improvements in the development of high fidelity numerical tools allows us to consider their use for gust load alleviation studies. The next steps to enhance these capabilities of the high fidelity numerical tools will focus on the coupling of a flight mechanics model with elsA in order to carry out unrestrained closed-loop control simulations with active devices.

## 8 ACKNOWLEDGEMENT

A part of the research leading to these results has received funding from the European Union’s Seventh Framework Programme (FP7/2007-2013) for the Clean Sky Joint Technology Initiative under grant agreement CSJU-GAM-SFWA-2008-001.

The studies presented in this article have been partially funded by Airbus, Safran, and ONERA which are co-owners of the software elsA.

## 9 REFERENCES


[1] Lepage, A., Amosse, Y. and Bellanger, M., *Gust Load alleviation : experimental validation of a gust generator for Wind Tunnel tests and progress status of the open loop campaign*, European Union's Clean Sky Joint Technology Initiative program - Smart Fixed Wing Aircraft Integrated Technology Demonstrator project - WP 1.2.4 Key deliverable D#7-2013, March 2013

[2] Brion, V., Lepage, A., Amosse, Y., Soulevant, D., Senecat, P., Abart, J. C., Paillart, P., *Generation of vertical gusts in a transonic wind tunnel*, Experiments in Fluids, Vol. 56 (7), p. 145, Jan. 2015

[3] Tang, D.M., Cizmas, P.G.A., Dowell E.H., *Experiments and Analysis for a gust generator in a wind tunnel* Journal of Aircraft, Vol. 33, N°1, Jan-Fev 1996

[4] S. Ricci and A. Scotti *Wind Tunnel Testing of an Active Controlled Wing under Gust Excitation* 49th AIAA/ASME/ASCE/AHS/ASC Structures, Structural Dynamics and Material Conference. 7- 10 April 2008, Schaumburg, IL, USA

[5] Silva, W. A., Vartio E. , Shimko, A., Kvaternik, R.G., Eure, K.W., Scott, R.C., *Development of Aeroservoelastic Analytical Models and Gust Load Alleviation Control Laws of a SensorCraft Wind-Tunnel Model Using Measured Data* IFASD 2007, International Forum on Aeroelasticity and Structural Dynamics, 18-20 Jun. 2007, Stockholm, Sweden

[6] Mai, H., Neumann, J., Hennings, H., *Gust Response : a validation experiment and preliminary numerical simulations*, International Forum on Aeroelasticity and Structural Dynamics 2011, International Forum of Aeroelasticity and Structural Dynamics 26-30 june 2011 Paris, France

[7] A.M. Rodde and J.P. Archambaud, *OAT15A Airfoil Data* AGARD ADVISORY REPORT N° 303 : " A selection of Experimental Test Cases for the Validation of CFD Codes"

[8] Cambier, L., Heib, S., Plot, S. , *The Onera elsA CFD software : input from research and feedback from industry*, Mechanics & Industry, 14(3): 159-174, doi:10.1051/meca/2013056, 2013

[9] Gazaix, M., Jolles, A., Lazareff, M., *The elsA Object-Oriented Computational tool for industrial applications*, 23rd Congress of ICAS, Toronto, Canada, 8-13 September, 2002.

[10] Girodroux-Lavigne, P., *Progress in steady/unsteady fluid-structure coupling with Navier-Stokes equations*, International Forum on Aeroelasticity and Structural Dynamics, 28 June – 1 July 2005, Munich, Germany.

[11] Dugeai, A., *Aeroelastic Developments in the elsA Code and Unsteady RANS Applications*, International Forum on Aeroelasticity and Structural Dynamics, 28 June – 1 July 2005, Munich, Germany.

[12] Girodroux-Lavigne, P., *Recent Navier-Stokes aeroelastic simulations using the elsA code for aircraft applications*, International Forum on Aeroelasticity and Structural Dynamics, 18-20 June 2007, Stockholm, Sweden.

[13] Sitaraman, J., Iyengar, V. S., and Baeder, J. D., 2003. *On field velocity approach and geometric conservation law for unsteady flow simulations*, 16th AIAA Computational Fluid Dynamics Conference, Orlando FL

[14] Liauzun, C., *Aeroelastic response to gust using CFD techniques*, Proceedings of 3rd Joint US-European Fluids Engineering Summer Meeting and 8th International

Conference on Nanochannels, Microchannels, and Minichannels, FEDSM2010-ICNMM2010, Montreal, Canada, August 2-4, 2010.

[15] Huvelin, F., Girodroux-Lavigne, P., Blondeau, C., *High fidelity numerical simulations for gust response analysis*, International Forum on Aeroelasticity and Structural Dynamics, 24-27 June 2013, Bristol, Great Britain.

[16] Lepage, A., Amosse Y., Le Bihan, D., Poussot-Vassal, C., *A complete experimental investigation of gust load from generation to active control*, International Forum on Aeroelasticity and Structural Dynamics, June 28-July 2 2015, Saint Petersburg, Russia

[17] Poussot-Vassal, C., Demourant, F., Lepage, A., Le Bihan, D., *Gust Load Alleviation: Identification, Control, and Wind Tunnel Testing of a 2-D Aeroelastic Airfoil*, IEEE Transactions on Control Systems Technology, Institute of Electrical and Electronics Engineers, 2016, p. 1-14

## COPYRIGHT STATEMENT